JGR Space Physics

COMMENTARY
10.1029/2021JA029211

**Key Points:**

- Atmospheric collisional energy degradation significantly affects precipitating electron distributions
- Backscatter influences ionospheric conductance and inner magnetospheric electrodynamics
- A framework for treating atmospheric backscatter in magnetospheric models is presented

**Correspondence to:**
G. V. Khazanov,
George.V.Khazanov@nasa.gov

**Citation:**
Khazanov, G. V., & Chen, M. W. (2021). Why atmospheric backscatter is important in the formation of electron precipitation in the diffuse aurora. *Journal of Geophysical Research: Space Physics*, *126*, e2021JA029211. https://doi.org/10.1029/2021JA029211

Received 5 FEB 2021
Accepted 7 MAY 2021



# Why Atmospheric Backscatter Is Important in the Formation of Electron Precipitation in the Diffuse Aurora

**George V. Khazanov[1] and Margaret W. Chen[2]**

[1]NASA Goddard Space Flight Center, Greenbelt, MD, USA, [2]The Aerospace Corporation, El Segundo, CA, USA

**Abstract** In addition to wave particle scattering in the magnetosphere, atmospheric backscatter of magnetospheric electrons is an important process that contributes to the formation of the precipitated electrons in the region of diffuse aurora. Two magnetically conjugate regions are involved in a complex magnetosphere-ionosphere (MI) particle and energy interplay. Based on synthesizing previous theoretical/modeling studies and experimental evidence, we demonstrate the need for improving the quantification of magnetospheric electrons backscatter processes that can affect inner magnetospheric electrodynamics, transport and loss in a way that is not easily predicted. We discuss how these complex and energy-dependent MI coupled processes can be treated in magnetospheric modeling.

## 1. Introduction

Magnetic storms and substorms result from a complex interaction of the solar wind with the Earth's magnetosphere. They reconfigure the near-Earth geospace environment and cause major increases in energetic particle precipitation in the auroral zone, making them an important component of space weather. The average integrated number flux of the precipitating auroral ions is typically 1 to 2 orders of magnitude less than that of the precipitating auroral electrons (Hardy et al., 1989) and precipitation of <∼30 keV electrons accounts for ∼80% of auroral energy into the ionosphere (Newell et al., 2009). Therefore, the flux formation of precipitating electrons is the focus in this paper.

There are three main auroral electron precipitation mechanisms: wave scattering of plasma sheet electrons into the loss cone; sometimes called diffuse aurora, acceleration by interactions with Alfvén waves; broadband or Alfvén aurora, and acceleration due to a quasi-static parallel electric field; monoenergetic or discrete aurora. Distributions of diffuse auroral electron fluxes precipitating downward into the ionosphere are often well represented by Maxwellian, kappa or Gaussian distributions (e.g., McIntosh & Anderson, 2014; Newell et al., 2009; 2010; Wing et al., 2013) that are similar to their near equatorial conjugate magnetospheric distribution (e.g., Meng et al., 1979; Weiss et al., 1997). Broadband precipitating auroral electrons exhibit a broad energy spectrum that may result from electron and dispersive Alfvén wave interactions (Chaston et al., 2002, 2003, 2008; Lessard et al., 2006). Inverted V acceleration or electrons that have been accelerated downward by a quasi-static field-aligned electric field may be associated with upward field-aligned currents (FACs) (e.g., Knight, 1973; Lyons, 1980; Johnson & Wing, 2015; Wing & Johnson, 2015). From analysis of Fast Auroral SnapshoT (FAST) energy spectra, Dombeck et al. (2018) found that intense electron precipitation events are frequently caused by a combination of two or more of the aforementioned mechanisms. For the purpose of aiding in conceptual understanding, we refer broadly to these processes as the *first step*.

Some of the electrons that precipitate into the atmosphere will backscatter into the magnetosphere. As "primary" electrons in the loss cone enter the atmosphere, impact ionization, and collisions of neutrals cause their energy degradation toward lower energies and production of secondary electrons. The mixed population of secondary and primary electrons cascade toward lower energies and some of the electrons can escape back to the magnetosphere, hence the term backscatter. Escaping electrons traveling upward from the ionosphere can be trapped in the magnetosphere, as they travel inside the loss cone, by interactions with different kinds of plasma waves or by Coulomb collisions with the cold plasma. Some of the primary precipitating electrons of magnetospheric origin are backscattered back into the magnetosphere, resulting in multiple backscatters between magnetically conjugate atmospheres. To aid in conceptual understanding, we refer to the backscattering processes and complex magnetosphere-ionosphere (MI) coupling of electrons

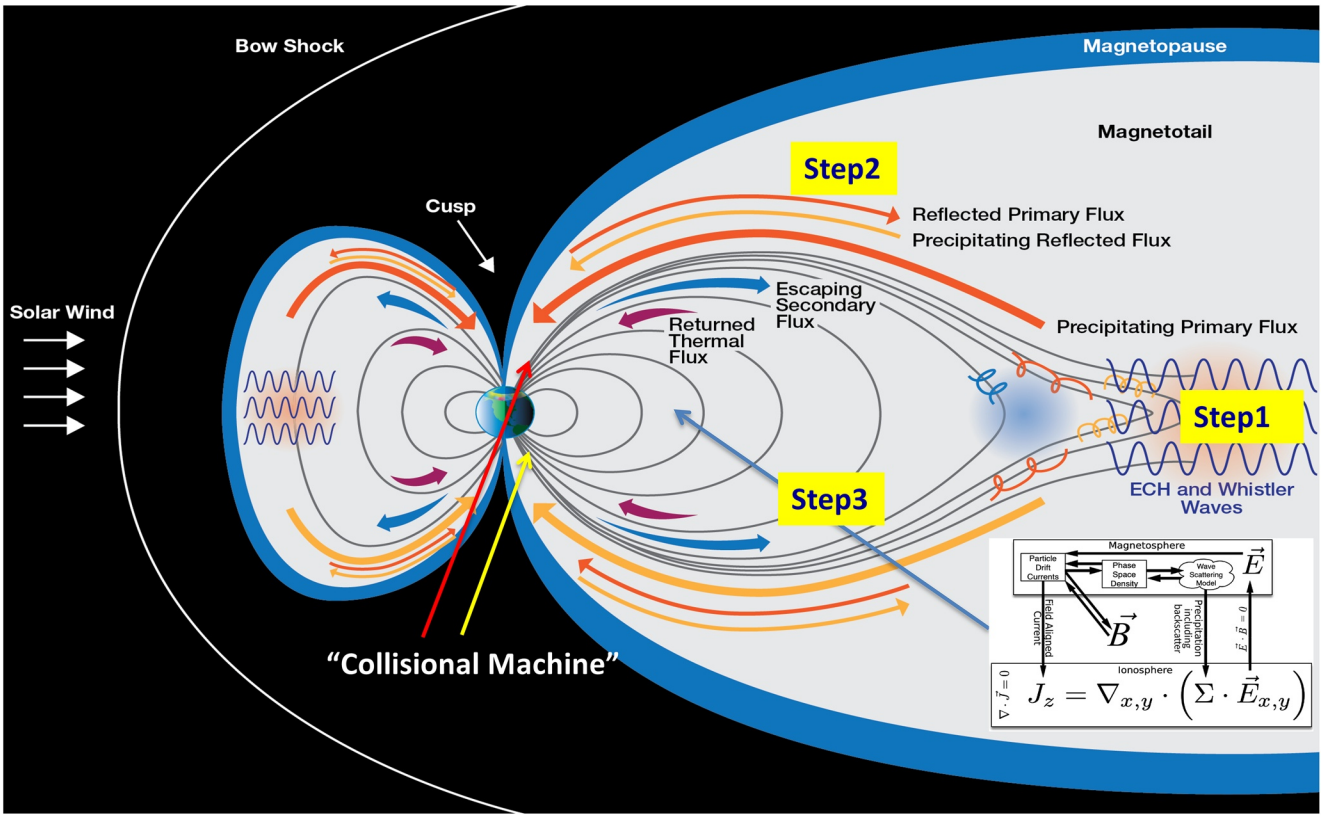


**Figure 1.** Schematic illustration of Magnetosphere-Ionosphere precipitated electron dynamic in the SuperThermal Electron Transport code.

in the loss cone as the *second step* (see Figure 1). The MI coupling of precipitating electrons has been calculated using the SuperThermal Electron Transport (STET) code that includes the full solution of the Boltzmann-Landau kinetic equation for the superthermal electrons, derived by Khazanov (1980; 2010). STET has been progressively improved upon and used to study electron precipitation phenomena in the diffuse auroral (Khazanov et al., 2015; 2017a; 2017b; Khazanov, Glocer et al., 2016; Khazanov, Himwich et al., 2016). Results of electron multiple backscatters computed by the STET code have been experimentally validated by Samara et al. (2017) in their case study of a pulsating auroral event imaged optically at high time resolution. STET simulations were also successfully compared to FAST (Khazanov, Himwich et al., 2016) and DMSP (Wing et al., 2019) observations. Additional evidence of MI precipitated electron energy interplay in aurora were discussed in recent experimental studies by Shen et al. (2020) and Artemyev et al. (2020).

Despite the complexity of there being multiple types of auroral electron precipitation, the diffuse aurora is a major component of that precipitation. Diffuse aurora is typically concentrated on the midnight to morning side over a broad latitudinal range. Scattering of low-energy (0.1–30 keV) electrons by waves in the central plasma sheet largely causes precipitation into the loss cone (Eather & Mende, 1971). For several decades there was controversy over which waves cause scattering into the loss cone (Belmont et al., 1983; Horne & Thorne, 2000; Horne et al., 2003; Johnstone et al., 1993; Kennel et al., 1970; Lyons, 1974; 1984; Meredith et al., 2000; 2009; Roeder & Koons, 1989): electron cyclotron harmonic (ECH) or whistler mode chorus waves. Thorne et al. (2010) found that chorus can scatter most electrons as they drift within the Earth's inner magnetosphere, leading to observed pancake distributions (Meredith et al., 1999) that can account for the global morphology of the diffuse aurora (Newell et al., 2009; Petrinec et al., 1999). Whistler chorus is reported to be effective for producing diffuse aurora at geocentric distances $r \leq 8\ R_E$ (Ni et al., 2008; Ni, Thorne, Horne et al., 2011; Ni, Thorne, Meredith et al., 2011) whereas ECH is effective at $r \geq 8\ R_E$ (Ni et al., 2012). The downward precipitation of "primary" electrons caused by wave scattering is illustrated schematically in Figure 1.

Like all precipitation, diffuse auroral electron precipitation which results from magnetospheric wave-electron interactions produces backscatter, alters the ionospheric conductance and affects inner magnetospheric electrodynamics. The electrodynamics potentially influences the formation of the plasmasphere (Huba & Krall, 2013), ring current (Chen, 2020; Chen, Lemon, Guild et al., 2015; Chen, Lemon, Orlova et al., 2015; Ebihara, 2016; Fok, 2020; Jordanova, 2020), and radiation belt seed population (Khazanov et al., 2004). A conceptual *third step* that involves a framework for using the diffuse precipitating electrons to calculate the inner magnetospheric electrodynamics, namely the self-consistent electric and magnetic fields that influence particle transport and loss including the primary precipitation is introduced and discussed in this paper.

The focus of this commentary is to clarify the great importance of atmospheric backscatter on electron precipitation in the diffuse aurora including pointing out the importance of the energy cascade associated with atmospheric albedo that was omitted in the discussion of Liemohn (2020), and to discuss how to treat complex diffuse electron precipitation processes, that are often oversimplified, in numerical inner magnetospheric models.

## 2. Magnetosphere-Ionosphere Interplay

### 2.1. Atmospheric Albedo

The atmospheric multiple backscatter phenomena (Step 2) that we are elucidating is an important element in the formation of electron precipitation. We consider the physics of this process by relating it to albedo. The classical definition of albedo from astrophysical research is the fraction of light that is reflected by a body or surface. It is commonly used in astronomy to describe the reflective properties of planets, satellites, and asteroids. Precipitated into the atmosphere, electrons can be reflected/backscatter by elastic collisions with the neutral atmosphere and this kind of reflectivity also was called albedo in the classical paper by Banks et al. (1974). Analyzing his auroral precipitation results, Banks et al. wrote "It appears that the albedo can range from 20% to 100%. However, it is necessary to remember that the upward flux is composed of energy degraded and scattered primaries as well as secondary particles." The same exact effect was discovered in the simulation by Lejeune (1979) who noticed that photoelectron fluxes escaping from the dark hemisphere can exceed the precipitated photoelectron fluxes that were coming from the illuminated hemisphere. Such an effect has been experimentally verified by Richards and Peterson (2008) and confirmed by Khazanov, Himwich et al. (2016) in their STET code simulations.

The formation of the atmospheric albedo is a complicated energy interplay process (Khazanov et al., 2014; 2020). For example, the 1 keV precipitating electron flux measured at the upper ionospheric altitude also includes the degraded high-energy electron population that came from the local or/and conjugate atmospheres. That is why the "effective" albedos of these fluxes are much higher that the "conventional" one, as it is shown in Figure 9.9 of (Khazanov, Glocer et al., 2016). As a result, the precipitated electron fluxes that build up between the magnetosphere and ionosphere (e.g., see Figure 1 of Khazanov et al., 2019) are higher than the fluxes that are driven only by magnetospheric processes.

Recently Liemohn (2020) misrepresented the idea of MI coupling of precipitating electrons in the diffuse aurora discussed by Khazanov et al. (2018) and provided an overly simplified and unrealistic multiple backscatter calculation of electron precipitated fluxes in equations (3) and (4) of his paper. His equations are based on the "conventional" albedo; $r$ reflection coefficient considering a single electron energy. The equations erroneously do not take into account a realistic electron energy spectra (e.g., Maxwellian, Kappa, or Guassian) and neglects the important energy cascade effects pointed out by the theoretical classical studies of Banks et al. (1974) and Lejeune (1979), and by Richards and Peterson (2008) in more recent experimental and theoretical FAST-based studies.

### 2.2. Energy Cascade Effects

Energy cascade effects on the precipitating electron flux distribution can be illustrated by considering that an arbitrary electron flux energy spectrum at an upper ionospheric location can be represented as a superposition of multiple monoenergetic flux energy spectra. Let us then consider the degradation of a single

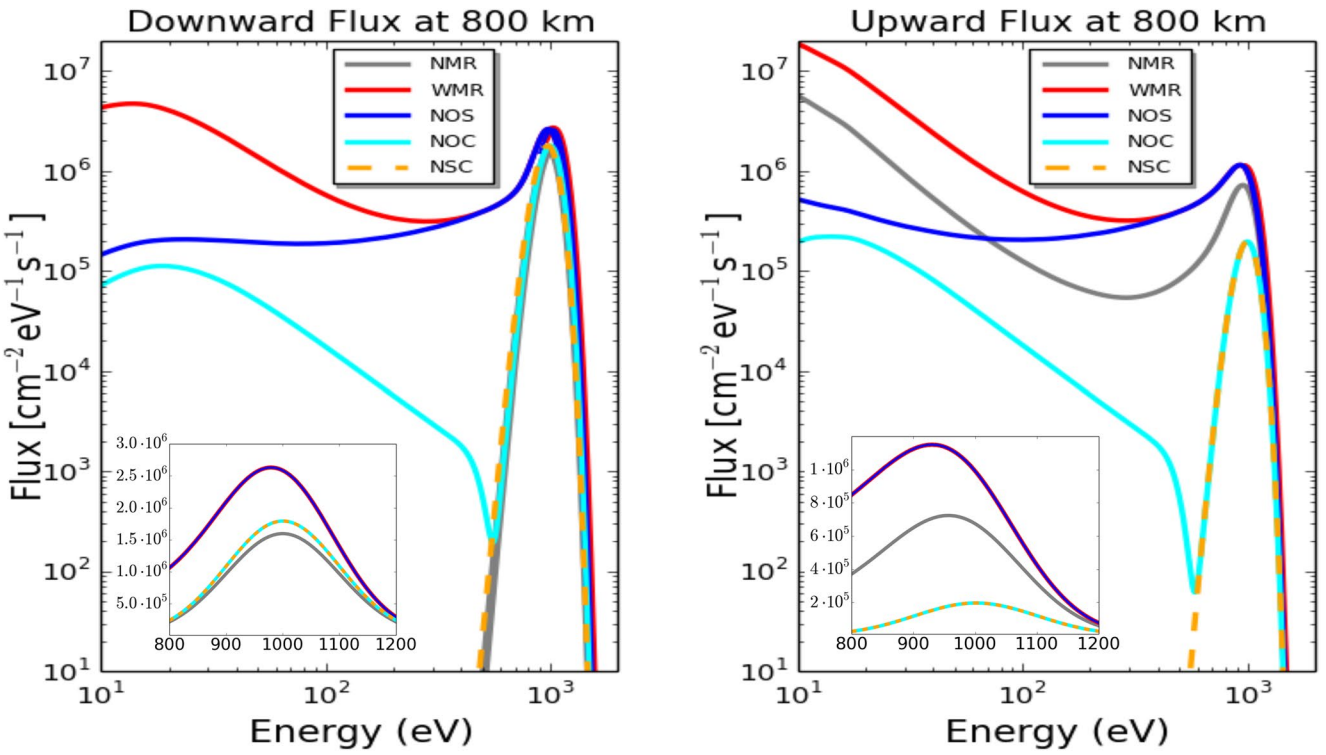


**Figure 2.** STET code simulation of 1 keV electron monoenergetic flux using different collisional processes turning "on" and "off," in order to demonstrate the important role of nonelastic collisional processes in the formation of electron precipitation in the diffuse aurora. In the insert panels, the red, and blue curves nearly overlap.

monoenergetic electron flux energy spectrum (shown as the gray NMR curve in Figure 2) in the energy range of 400 eV and 2 keV with a maximum value at 1 keV. We applied this spectrum at an altitude of 800 km and a magnetic local time (MLT) of 0 in both magnetically conjugate regions in the STET model. The resulting steady-state energy distributions of downward (left panel) and upward (right panel) electron fluxes in the ionosphere computed from STET in Figure 2 show the effects of energy cascade that are missing in the analysis presented by Liemohn (2020). The steady-state distributions are calculated by setting the time derivative of the energy distribution function in the kinetic equation equal to zero and converging iteratively to a solution (Khazanov, 2010). The red solid curves labeled WMR correspond to the case when all processes that produce precipitating and escaping electrons are taken in to account. The dark blue curves correspond to the "NOS" case when secondary electron production is completely removed from the simulations and only the effects of primary electrons are included. Comparison of the dark blue and red curves reveal that the secondary electrons (SE) enhance the downward and upward fluxes at energies below about 300 eV. These fluxes at 10 eV, for example, increase by factors of 40 when secondary electron production is taken into account.

The light blue line in Figure 2 (NOC notation) represents the case when the energy cascading processes are completely ignored in the simulations of SE fluxes. In this case, it is the production of secondary electrons that contribute to fluxes at energies below 400 eV. As one can see from the simulation results, the primary degraded 1 keV monoenergetic electrons play a key role in the formation of the low energy fluxes down to energies of a few tens of eV. Such a conclusion is relevant for the both, downward and upward electron energy fluxes that are presented in Figure 2. Ignoring both, the secondary electron production and the cascading processes of primary and secondary electrons (case NSC) completely removes the low energy part of the spectra from the simulation results leaving only the energy domain of the injected primary magnetospheric electrons above of 400 eV. This is the scenario that corresponds to the discussion presented by Liemohn (2020) in his formulas (3) and (4) when the nonelastic processes are completely ignored from consideration.

Because some of the energy flux curves that are presented in Figure 2 are very close to each other in the vicinity of 1 keV, portions of the electron spectra at energies of 800 and 1,200 eV were presented on a magnified scale are shown as inserted panels of Figure 2. The peak electron flux value with all the collisional processes (red curve) included is a factor of 1.7 higher than the initial flux peak (gray curve). STET simulations of another single monoenergetic spectrum at an energy of 20 keV with all collisional processes turned on (not shown here) resulted in a 3-fold increase in the peak electron flux value compared to the initial peak value. The superposition of several monoenergetic spectra from 1 to 30 keV would provide further enhancement to the electron flux at energies below 1 keV. These results clearly demonstrate the dramatic role of the energy cascading processes in the formation of electron precipitation that was missing in the discussion by Liemohn (2020).

### 2.3. Non-Steady-State Features

The analysis that we present in this Commentary focuses on diffuse aurora and has not yet been extended to explain intense electron precipitation events caused by precipitation mechanisms such as acceleration due to Alfven waves or parallel electric fields or a combination of these and diffuse auroral scattering as discussed by Dombeck et al. (2018) who analyzed high-time resolution FAST electron data. Nevertheless, examining the dynamic features of the diffuse auroral electron precipitation spectra may help with interpreting observed electron distribution fluxes in the auroral region.

The left panel of Figure 3 shows the time evolution of the formation of downward directional electron fluxes for $L = 6$ (MLT = 0) at an altitude of 800 km calculated from the time-dependent STET code. For this example, it is assumed that the initial electron distribution function in the energy range of 600 eV–10 keV is a Maxwellian given by

$$\Phi\left(E\right) = CEexp\left(-\frac{E}{E_0}\right), \tag{1}$$

where the characteristic energy $E_0$ is 2 keV and $C$ is chosen so that the total energy flux into both magnetically conjugate regions equals 2 erg cm$^{-2}$ s$^{-1}$. Figure 3, in the first panel, illustrates this process and shows the formation of downward directional fluxes for $L = 6$ at an altitude of 800 km at different time stages of electron precipitation. The ratio of upward to downward fluxes and its dynamic development is shown in the second panel of Figure 3. There is a persistent asymmetry (higher upward fluxes) that is strong early on and becomes less pronounced by the time the simulations reach steady-state conditions.

We show these results in the reference to the new, very interesting methodology, for identifying electron precipitation mechanisms in Earth's auroral zone, presented by Dombeck et al. (2018), that utilizes FAST measurements of upward energy and pitch angle spectra. As shown in Figure 3, considerations of the temporal evolution of the electron energy spectra should be taken into account when identifying electron precipitation mechanisms.

## 3. MI Electrodynamic Coupling of Precipitated Electrons

Diffuse auroral electron precipitation including backscatter affects ionospheric conductance and inner magnetospheric electrodynamics. The theory describing electrodynamic coupling between the ionospheric electric field, FACs, perpendicular currents from particle drifts, particle pressure, and inner magnetospheric electric $E$ and magnetic $B$ fields was pioneered by Vasyliunas (1970) and Wolf (1970). The current continuity equation ($\nabla \cdot \boldsymbol{J} = 0$), Ohm's law ($J_z = \nabla_{x,y} \cdot \left(\boldsymbol{\Sigma} \cdot \boldsymbol{E}_{x,y}\right)$) that relates field aligned currents $J_z$ to the ionospheric conductance $\sum$ and electric field, and the electrostatic condition ($\boldsymbol{E} \cdot \boldsymbol{B} = 0$) to map the ionospheric electric potentials along magnetic field lines are used to model electrodynamics (see flow chart in Figure 1). The electrodynamics would be calculated within a kinetic model that treats inner magnetospheric particle drifts and loss including precipitation such as in the Rice Convection Model – Equilibirum (RCM-E) (Chen et al., 2019; Lemon et al., 2004).

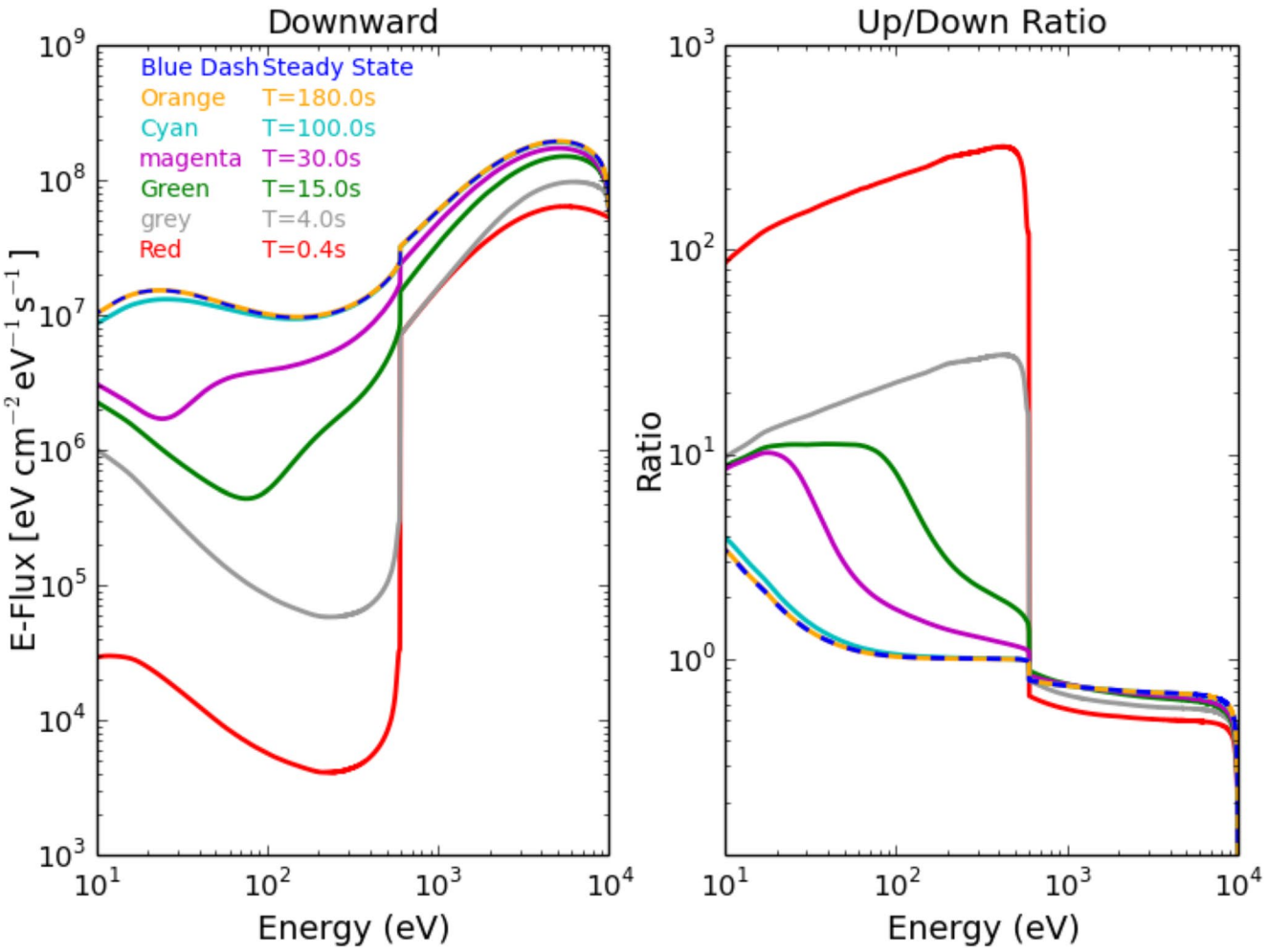


**Figure 3.** The non-steady-state precipitating electron energy flux formation and the ratio between upward and downward fluxes for the characteristic energy $E_0 = 2$ keV at the different time stages.

The Robinson et al. (1987) formulas relate the integrated precipitating electron energy flux and the mean electron energy to the Hall and Pedersen conductance and have been used in numerous models kinetic (e.g., Chen et al., 2019; Perlongo et al., 2017; Toffoletto et al., 2003) and magnetohydrodynamic (e.g., Lotko et al., 2014; Raeder et al., 2001; Wiltberger et al., 2009; Zhang et al., 2015) models. Liemohn (2020) in his commentary wrote "Perhaps the biggest concern with the Robinson formulas is that they are based on only three days of incoherent radar data of moderate activity." This statement is a misrepresentation of the Robinson et al. (1987) study in which incoherent radar data was not used to derive the Robinson formulas but rather for an example to demonstrate how the formulas can be applied. The Robinson formulas, were based on model calculations performed using the energy deposition code by Rees (1963), and the method of computing the height profile electron density between 80 and 200 km altitude validated by Vondrak and Robinson (1985).

We believe that the Robinson formulas are handy approximations of the height-integrated conductance. As Liemohn (2020) has pointed out, care is needed when applying the Robinson formulas. This includes but is not limited to a careful selection of the inputs such as the appropriate energy range of the electron spectra as described in Khazanov et al. (2018, 2019).

In the past, many magnetospheric models had recognized that a fraction of simulated precipitating electron flux into the ionosphere would be backscattered (e.g., Chen and Schulz (2001a; 2001b); Chen et al., 2005; 2012; Sazykin et al., 2005; Wolf et al., 1982) but the fractions imposed were constant in time and

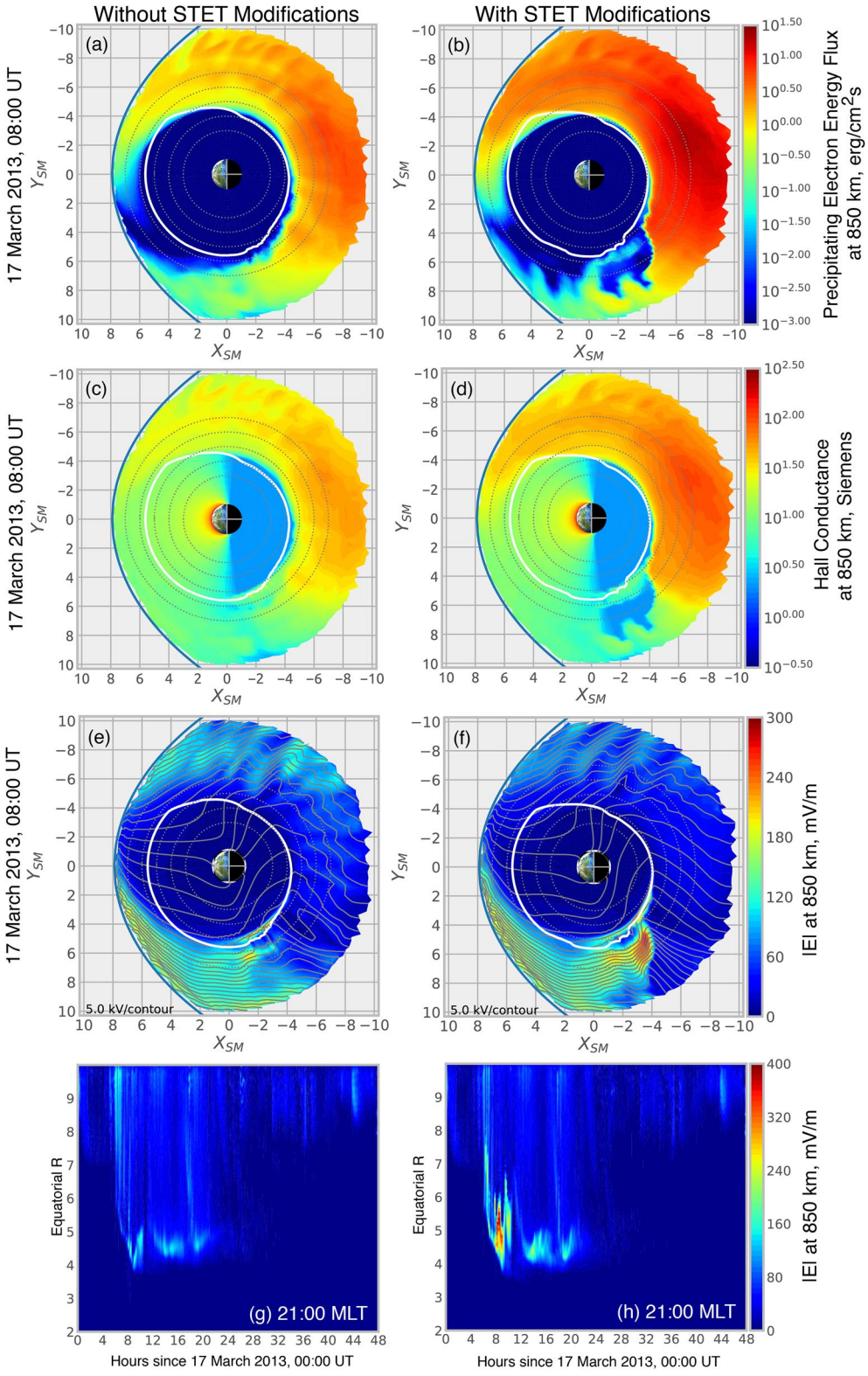


**Figure 4.** Panels reproduced from figures from Khazanov et al. (2019). For 08:00 UT on March 17, 2013: The simulated (a) and (b) precipitating electron flux, (c) and (d) Hall conductance, (e) and (f) electric intensity |E| at 850 km, mapped to the equatorial plane without, and with SuperThermal Electron Transport (STET) modifications. (g) and (h) The equatorial radial profiles at 21:00 MLT of the simulated |E| at 850 km versus hours after March 17, 2013, 00:00 UT without, and with STET modifications. The white and gray curves correspond to the Rice Convection Model – Equilibirum plasmapause and the 2.5 -Siemen contour, respectively. MLAT = magnetic latitude; MLT = magnetic local time.

did not include the energy cascade effects discussed in Section 2. For studying phenomena with time resolution less than ~3 min, electron precipitation including backscatter processes can be calculated by a two-way coupling of primary electron precipitation and the STET model. For time resolution greater than ~3 min, it is reasonable to use expressions provided in Khazanov et al. (2019) that modify simulated primary precipitating electron integrated flux and mean energy based on steady-state solutions of STET.

The approach of steady-state STET modification of the primary electron precipitation distributions simulated by Aerospace's version latest version of the Rice Convection Model-Equilibrium (Chen et al., 2019) was used to model the large March 17, 2013 geomagnetic storm because the magnetic and electric fields were updated every 5 min. The results revealed that the MI coupled electron precipitation effects on conductance are quantitatively significant but not predictable because of the complex IM electrodynamics (Khazanov et al., 2019). In the auroral region, STET modifications enhance the simulated integrated precipitating electron fluxes from pre-midnight to noon but reduce the fluxes drastically between dusk and pre-midnight early in the storm main phase (see Figure 4). The simulated Hall and Pedersen (not shown) conductance with the STET modifications vary similarly with equatorial geocentric distance and magnetic local time (MLT) as the precipitating electron energy fluxes during the storm. Early in the storm main phase, a sharp boundary between high and low conductance (described as a "hole") on the dusk side forms because a large proportion of the electron population are precipitated before they can reach dusk as their drift speed slows down near kinks in the equatorial equipotentials. The conductance hole results in larger **E** x **B** drifts in the dusk region including subauroral polarization streams (SAPS). In contrast, where the simulated auroral conductance is enhanced, there is a weakening of the electric field. Because it is easier to drive currents through the ionosphere where there is high conductance, this results in less feedback to the electric field. Effectively, less shielding of the electric field occurred at lower MLATs or equatorial geocentric distances in the enhanced auroral region with the STET modifications than without. Reduced shielding in this region enabled ions, with relatively longer lifetimes than electrons to be transported to lower $L$ values resulting in enhancement of the ring current perturbation magnetic field.

The example presented here is just one application of using the MI coupled electron precipitation fluxes to calculate the inner magnetospheric electrodynamics and its effects (step 3). The STET-modified formulas provided in Khazanov et al. (2018; 2019) can be used to account for atmospheric backscatter effects on simulated primary electron fluxes in other magnetospheric models or coupled kinetic-magnetohydrodynamic (MHD) models to investigate formation of the plasmasphere, radiation belt seed population, and ionospheric heavy ions outflows.

## 4. Concluding Remarks

The precipitation of diffuse auroral electrons into the ionosphere involves complex and coupled processes but for the sake of conceptual understanding can be described by a cyclical three-step process. The first step is the initiation of electron precipitation into both magnetically conjugate points from the Earth's plasma sheet via wave-particle interactions. The second step consisting of the multiple atmospheric backscatters of electrons at the two magnetically conjugate points within the loss cone. The third step is to use the MI coupled precipitated electron fluxes to calculate the MI electrodynamics that affects particle transport and wave growth. Magnetospheric models that include MI coupling should include atmospheric backscatter of diffuse auroral electron precipitation because these processes significantly affect the simulated electron flux energy distribution, ionospheric conductance, and inner magnetospheric electrodynamics.

**Acknowledgments**
G. V. Khazanov was supported by NASA HTMS program under award of 80NSSC20K1276, and LWS Program under the awards 80NSSC19K0080 and 80NSSC20K1817. The research work of M. W. Chen at The Aerospace Corporation was supported by the NSF grant AGS 1602862, the Aerospace Technical Investment Program, and the NASA grant NNH19ZDA001N-HGIO.

## Data Availability Statement

This is a theoretical study and all information that we presented here can be found in the papers by Chen et al. (2015), Chen et al. (2019), Khazanov et al. (2018), and Khazanov et al. (2019).

## References

Artemyev, A. V., Zhang, X. J., Angelopoulos, V., Mourenas, D., Vainchtein, D., Shen, Y., et al. (2020). Ionosphere feedback to electron scattering by equatorial whistler mode waves. *Journal of Geophysical Research: Space Physics*, *125*, e2020JA028373. https://doi.org/10.1029/2020JA028373

Banks, P. M., Chappell, C. R., & Nagy, A. F. (1974). A new model for the interaction of auroral electrons with the atmosphere: Spectral degradation, backscatter, optical emission, and ionization. *Journal of Geophysical Research*, *79*, 1459–1470. https://doi.org/10.1029/JA079i010p01459

Belmont, G., Fontaine, D., & Canu, P. (1983). Are equatorial electron cyclotron waves responsible for diffuse auroral electron precipitation? *Journal of Geophysical Research*, *88*, 9163–9170. https://doi.org/10.1029/JA088iA11p09163

Belmont, G., Fontaine, D., & Canu, P. (1984). Reply [to "Comment on 'Are equatorial electron cyclotron waves responsible for diffuse auroral electron precipitation?' by G. Belmont, D. Fontaine, and P. Canu"]. *Journal of Geophysical Research*, *89*, 7591–7592. https://doi.org/10.1029/JA089iA09p07591

Chaston, C., Bonnell, J., McFadden, J. P., Carlson, C. W., Cully, C., Le Contel, O., et al. (2008). Turbulent heating and cross-field transport near the magnetopause from THEMIS. *Geophysical Research Letters*, *35*, L17S08. https://doi.org/10.1029/2008GL033601

Chaston, C. C., Bonnell, J. W., Carlson, C. W., McFadden, J. P., Ergun, R. E., & Strangeway, R. J. (2003). Properties of small-scale Alfvén waves and accelerated electrons from FAST. *Journal of Geophysical Research*, *108*, 8003. https://doi.org/10.1029/2002JA009420

Chaston, C. C., Bonnell, J. W., Peticolas, L. M., Carlson, C. W., McFadden, J. P., & Ergun, R. E. (2002). Driven Alfvén waves and electron acceleration. *Geophysical Research Letters*, *29*, 1535. https://doi.org/10.1029/2001gl013842

Chen, M. W. (2005). Storm time distributions of diffuse auroral electron energy and X-ray flux: Comparison of drift-loss simulations with observations. *Journal of Geophysical Research*, *110*(A3), A03210. https://doi.org/10.1029/2004JA010725

Chen, M. W. (2020). Ring current development. In V. Jordanova, R. Ilie, & M. W. Chen (Eds.), *Ring current investigations: The Quest for space weather prediction* (pp. 153–180). Amsterdam, The Netherlands: Elsevier, https://doi.org/10.1016/B978-0-12-815571-4.00005-6

Chen, M. W., Lemon, C. L., Guild, T. B., Keesee, A. M., Lui, A., Goldstein, J., et al. (2015). Effects of modeled ionospheric conductance and electron loss on self-consistent ring current simulations during the 5-7 April 2010 storm. *Journal of Geophysical Research: Space Physics*, *120*, 5355–5376. https://doi.org/10.1002/2015JA021285

Chen, M. W., Lemon, C. L., Guild, T. B., Schulz, M., Roeder, J. L., & Le, G. (2012). Comparison of self-consistent simulations with observed magnetic field and ion plasma parameters in the ring current during the 10 August 2000 magnetic storm. *Journal of Geophysical Research*, *117*, A09232. https://doi.org/10.1029/2012JA017788

Chen, M. W., Lemon, C. L., Hecht, J., Sazykin, S., Wolf, R. A., Boyd, A., & Valek, P. (2019). Diffuse auroral electron and ion precipitation effects on RCM-E comparisons with satellite data during the 17 March 2013 storm. *Journal of Geophysical Research: Space Physics*, *124*, 4194–4216. https://doi.org/10.1029/2019JA026545

Chen, M. W., Lemon, C. L., Orlova, K., Shprits, Y., Hecht, J., & Walterscheid, R. L. (2015). Comparison of simulated and observed trapped and precipitating electron fluxes during a magnetic storm. *Geophysical Research Letters*, *42*, 8302–8311. https://doi.org/10.1002/2015GL065737

Chen, M. W., & Schulz, M. (2001a). Simulations of diffuse aurora with plasma sheet electrons in pitch angle diffusion less than everywhere strong. *Journal of Geophysical Research*, *106*(A12), 28949–28966. https://doi.org/10.1029/2001JA000138

Chen, M. W., & Schulz, M. (2001b). Simulations of storm time diffuse aurora with plasmasheet electrons in strong pitch angle diffusion. *Journal of Geophysical Research*, *106*, 1873–1886. https://doi.org/10.1029/2000ja000161

Dombeck, J., Cattell, C., Prasad, N., Meeker, E., Hanson, E., & McFadden, J. (2018). Identification of auroral electron precipitation mechanism combinations and their relationships to net downgoing energy and number flux. *Journal of Geophysical Research: Space Physics*, *123*, 10064–10089. https://doi.org/10.1029/2018JA025749

Eather, R. H., & Mende, S. B. (1971). Airborne observations of auroral precipitation patterns. *Journal of Geophysical Research*, *76*, 1746–1755. https://doi.org/10.1029/JA076i007p01746

Ebihara, Y. (2016). *Ring current, space weather fundamentals*. In G. V. Khazanov (Ed.), London New York: CRC Press.

Fok, M.-C. (2020). Chapter 7: Cross-regional coupling. In V. Jordanova, R. Ilie, & M. W. Chen (Eds.), *Cross-regional coupling, ring current investigations: The Quest for space weather prediction* (pp. 225–244). Amsterdam, The Netherlands: Elsevier. https://doi.org/10.1016/B978-0-12-815571-4.00007-X

Hardy, D. A., Gussenhoven, M. S., & Brautigam, D. (1989). A statistical model of auroral ion precipitation. *Journal of Geophysical Research*, *94*, 370–392. https://doi.org/10.1029/JA094iA01p00370

Horne, R. B., & Thorne, R. M. (2000). Electron pitch angle diffusion by electrostatic electron cyclotron harmonic waves: The origin of pancake distributions. *Journal of Geophysical Research*, *105*, 5391–5402. https://doi.org/10.1029/1999JA900447

Horne, R. B., Thorne, R. M., Meredith, N. P., & Anderson, R. R. (2003). Diffuse auroral electron scattering by electron cyclotron harmonic and whistler mode waves during an isolated substorm. *Journal of Geophysical Research*, *108*(A7), 1290. https://doi.org/10.1029/2002JA009736

Huba, J., & Krall, J. (2013). Modeling the plasmasphere with SAMI3. *Geophysical Research Letters*, *40*, 6–10. https://doi.org/10.1029/2012GL054300

Johnson, J. R., & Wing, S. (2015). The dependence of the strength and thickness of field-aligned currents on solar wind and ionospheric parameters. *Journal of Geophysical Research: Space Physics*, *120*, 3987–4008. https://doi.org/10.1002/2014JA020312

Johnstone, A. D., Walton, D. M., Liu, R., & Hardy, D. A. (1993). Pitch angle diffusion of low-energy electrons by whistler mode waves. *Journal of Geophysical Research*, *98*, 5959–5967. https://doi.org/10.1029/92JA02376

Jordanova, V. K. (2020). Chapter 6: Ring current decay. In V. Jordanova, R. Ilie, & M. W. Chen. (Eds.), *Ring current investigations: The Quest for space weather prediction* (pp. 181–223). Amsterdam, The Netherlands: Elsevier. https://doi.org/10.1016/B978-0-12-815571-4.00006-8

Kennel, C. F., Scarf, F. L., Fredricks, R. W., McGehee, J. H., & Coroniti, F. V. (1970). VLF electric field observations in the magnetosphere. *Journal of Geophysical Research*, *75*, 6136–6152. https://doi.org/10.1029/JA075i031p06136

Khazanov, G. V. (1980). *The kinetics of the electron plasma component of the upper atmosphere*. Moscow: Nauka. [English Translation: Washington, D. C., National Translation Center 80-50707, 1980].

Khazanov, G. V. (2010). *Kinetic theory of inner magnetospheric plasma*. (Vol. 372, p. 584). New York: Springer.

Khazanov, G. V., Chen, M. W., Lemon, C. L., & Sibeck, D. G. (2019). The magnetosphere-ionosphere electron precipitation dynamics and their geospace consequences during the 17 March 2013 storm. *Journal of Geophysical Research: Space Physics*, *124*, 6504–6523. https://doi.org/10.1029/2019ja026589

Khazanov, G. V., Glocer, A., & Chu, M. (2020). The Formation of electron heat flux in the region of diffuse aurora. *Journal of Geophysical Research: Space Physics*, *125*, e2020JA028175. https://doi.org/10.1029/2020ja028175

Khazanov, G. V., Glocer, A., & Himwich, E. W. (2014). Magnetosphere-ionosphere energy interchange in the electron diffuse aurora. *Journal of Geophysical Research: Space Physics*, *119*, 171–184. https://doi.org/10.1002/2013JA019325

Khazanov, G. V., Glocer, A., Sibeck, D. G., Tripathi, A. K., Detweiler, L. G., Avanov, L. A., & Singhal, R. P. (2016). Ionosphere-magnetosphere energy interplay in the regions of diffuse aurora. *Journal of Geophysical Research: Space Physics*, *121*(7), 6661–6673. https://doi.org/10.1002/2016ja022403

Khazanov, G. V., Himwich, E. W., Glocer, A., & Sibeck, D. (2016). The role of multiple atmospheric reflections in the formation of the electron distribution function in the diffuse aurora region. *AGU monograph, 215,"Auroral dynamics and space weather"*, pp. 115–130. https://doi.org/10.1002/9781118978719

Khazanov, G. V., Liemohn, M. W., Fok, M.-C., Newman, T. S., & Ridley, A. J. (2004). Stormtime particle energization with high temporal resolution AMIE potentials. *Journal of Geophysical Research*, *109*, A05209. https://doi.org/10.1029/2003JA010186

Khazanov, G. V., Robinson, R. M., Zesta, E., Sibeck, D. G., Chu, M., & Grubbs, G. A. (2018). Impact of precipitating electrons and magnetosphere-ionosphere coupling processes on ionospheric conductance. *Space Weather*, *16*, 829–837. https://doi.org/10.1029/2018SW001837

Khazanov, G. V., Sibeck, D. G., & Zesta, E. (2017a). Is diffuse aurora driven from above or below? *Geophysical Research Letters*, *44*, 641–647. https://doi.org/10.1002/2016GL072063

Khazanov, G. V., Sibeck, D. G., & Zesta, E. (2017b). Major pathways to electron distribution function formation in regions of diffuse aurora. *Journal of Geophysical Research: Space Physics*, *122*, 4251–4265. https://doi.org/10.1002/2017JA023956

Khazanov, G. V., Tripathi, A. K., Sibeck, D., Himwich, E., Glocer, A., & Singhal, R. P. (2015). Electron distribution function formation in regions of diffuse aurora. *Journal of Geophysical Research: Space Physics*, *120*, 9891–9915. https://doi.org/10.1002/2015ja021728

Knight, S. (1973). Parallel electric fields. *Planetary and Space Science*, *21*(5), 741–750. https://doi.org/10.1016/0032-0633(73)90093-7

Lejeune, G. (1979). "Two-stream" photoelectron distributions with interhemispheric coupling: A mixing of analytical and numerical methods. *Planetary and Space Science*, *27*, 561–576. https://doi.org/10.1016/0032-0633(79)90154-5

Lemon, C., Wolf, R. A., Hill, T. W., Sazykin, S., Spiro, R. W., Toffoletto, F. R., et al. (2004). Magnetic storm ring current injection modeled with the Rice Convection Model and a self-consistent magnetic field. *Geophysical Research Letters*, *31*(21), L21801. https://doi.org/10.1029/2004GL020914

Lessard, M. R., Lund, E. J., Jones, S. L., Arnoldy, R. L., Posch, J. L., Engebretson, M. J., & Hayashi, K. (2006). Nature of Pi1B pulsations as inferred from ground and satellite observations. *Geophysical Research Letters*, *33*, L14108. https://doi.org/10.1029/2006GL026411

Liemohn, M. W. (2020). The case for improving the Robinson formulas. *Journal of Geophysical Research: Space Physics*, *125*, e2020JA028332. https://doi.org/10.1029/2020JA028332

Lotko, W., Smith, R. H., Zhang, B., Ouellette, J. E., Brambles, O. J., & Lyon, J. G. (2014). Ionospheric control of magnetotail reconnection. *Science*, *345*(6193), 184–187. https://doi.org/10.1126/science.1252907

Lyons, L. R. (1974). Electron diffusion driven by magnetospheric electrostatic waves. *Journal of Geophysical Research*, *79*(4), 575–580. https://doi.org/10.1029/JA079i004p00575

Lyons, L. R. (1980). Generation of large-scale regions of auroral currents, electric potentials, and precipitation by the divergence of the convection electric field. *Journal of Geophysical Research*, *85*, 17–24. https://doi.org/10.1029/ja085ia01p00017

McIntosh, R. C., & Anderson, P. C. (2014). Maps of precipitating electron spectra characterized by Maxwellian and kappa distributions. *Journal of Geophysical Research: Space Physics*, *119*, 10116–10132. https://doi.org/10.1002/2014JA020080

Meng, C.-I., Mauk, B., & McIlwain, C. E. (1979). Electron precipitation of evening diffuse aurora and its conjugate electron fluxes near the magnetospheric equator. *Journal of Geophysical Research*, *84*, 2545–2558. https://doi.org/10.1029/JA084iA06p02545

Meredith, N. P., Horne, R. B., Johnstone, A. D., & Anderson, R. R. (2000). The temporal evolution of electron distributions and associated wave activity following substorm injections in the inner magnetosphere. *Journal of Geophysical Research*, *105*, 12907–12917. https://doi.org/10.1029/2000JA900010

Meredith, N. P., Horne, R. B., Thorne, R. M., & Anderson, R. R. (2009). Survey of upper band chorus and ECH waves: Implications for the diffuse aurora. *Journal of Geophysical Research*, *114*, A07218. https://doi.org/10.1029/2009JA014230

Meredith, N. P., Johnstone, A. D., Szita, S., Horne, R. B., & Anderson, R. R. (1999). "Pancake" electron distributions in the outer radiation belts. *Journal of Geophysical Research*, *104*, 12431–12444. https://doi.org/10.1029/1998ja900083

Newell, P. T., Sotirelis, T., & Wing, S. (2009). Diffuse, monoenergetic, and broadband aurora: The global precipitation budget. *Journal of Geophysical Research*, *114*, A09207. https://doi.org/10.1029/2009JA014326

Newell, P. T., Sotirelis, T., & Wing, S. (2010). Seasonal variations in diffuse, monoenergetic, and broadband aurora. *Journal of Geophysical Research*, *115*, A03216. https://doi.org/10.1029/2009JA014805

Ni, B., Liang, J., Thorne, R. M., Angelopoulos, V., Horne, R. B., Kubyshkina, M., et al. (2012). Efficient diffuse auroral electron scattering by electrostatic electron cyclotron harmonic waves in the outer magnetosphere: A detailed case study. *Journal of Geophysical Research*, *117*, A01218. https://doi.org/10.1029/2011JA017095

Ni, B., Thorne, R. M., Horne, R. B., Meredith, N. P., Shprits, Y. Y., Chen, L., & Li, W. (2011). Resonant scattering of plasma sheet electrons leading to diffuse auroral precipitation: 1. Evaluation for electrostatic electron cyclotron harmonic waves. *Journal of Geophysical Research*, *116*, A04218. https://doi.org/10.1029/2010JA016232

Ni, B., Thorne, R. M., Meredith, N. P., Horne, R. B., & Shprits, Y. Y. (2011). Resonant scattering of plasma sheet electrons leading to diffuse auroral precipitation: 2. Evaluation for whistler mode chorus waves. *Journal of Geophysical Research*, *116*, A04219. https://doi.org/10.1029/2010JA016233

Ni, B., Thorne, R. M., Shprits, Y. Y., & Bortnik, J. (2008). Resonant scattering of plasma sheet electrons by whistler-mode chorus: Contribution to diffuse auroral precipitation. *Geophysical Research Letters*, *35*, L11106. https://doi.org/10.1029/2008GL034032

Perlongo, N. J., Ridley, A. J., Liemohn, M. W., & Katus, R. M. (2017). The effect of ring current electron scattering rates on magnetosphere-ionosphere coupling. *Journal of Geophysical Research: Space Physics*, *122*, 4168–4189. https://doi.org/10.1002/2016JA023679

Petrinec, S. M., Chenette, D. L., Mobilia, J., Rinaldi, M. A., & Imhof, W. L. (1999). Statistical X ray auroral emissions - PIXIE observations. *Geophysical Research Letters*, *26*(11), 1565–1568. https://doi.org/10.1029/1999GL900295

Raeder, J., Wang, Y., & Fuller-Rowell, T. J. (2001). Geomagnetic storm simulation with a coupled magnetosphere-ionosphere-thermosphere model. *Space Weather*, *125*, 377–384. https://doi.org/10.1029/GM125p0377

Rees, M. H. (1963). Auroral ionization and excitation by incident energetic electrons. *Planetary and Space Science*, *11*, 1209–1218. https://doi.org/10.1016/0032-0633(63)90252-6

Richards, P. G., & Peterson, W. K. (2008). Measured and modeled backscatter of ionospheric photoelectron fluxes. *Journal of Geophysical Research*, *113*, A08321. https://doi.org/10.1029/2008JA013092

Robinson, R. M., Vondrak, R. R., Miller, K., Dabbs, T., & Hardy, D. (1987). On calculating ionospheric conductances from the flux and energy of precipitating electrons. *Journal of Geophysical Research*, *92*(A3), 2565–2569. https://doi.org/10.1029/JA092iA03p02565

Roeder, J. L., & Koons, H. C. (1989). A survey of electron cyclotron waves in the magnetosphere and the diffuse auroral electron precipitation. *Journal of Geophysical Research*, *94*, 2529–2541. https://doi.org/10.1029/JA094iA03p02529

Samara, M., Michell, R. G., & Khazanov, G. V. (2017). First optical observations of interhemispheric electron reflections within pulsating aurora. *Geophysical Research Letters*, *44*(6), 2618–2623. https://doi.org/10.1002/2017gl072794

Sazykin, S., Spiro, R. W., Wolf, R. A., Toffoletto, F. R., Tsyganenko, N., Goldstein, J., & Hairston, M. R. (2005). Modeling inner magnetospheric electric fields: Latest self-consistent results. In T. I. Pulkkinen, N. A. Tsyganenko, & R. H. W. Friedel (Eds.), Geophysical monograph series (Vol. 155, pp. 263–269). American Geophysical Union. https://doi.org/10.1029/155GM28

Shen, Y., Artemyev, A., Zhang, X. J., Vasko, I. Y., Runov, A., Angelopoulos, V., & Knudsen, D. (2020). Potential evidence of low-energy electron scattering and ionospheric precipitation by time domain structures. *Geophysical Research Letters*, *47*, e2020GL089138. https://doi.org/10.1029/2020GL089138

Thorne, R. M., Ni, B., Tao, X., Horne, R. B., & Meredith, N. P. (2010). Scattering by chorus waves as the dominant cause of diffuse auroral precipitation. *Nature*, *467*, 943–946. https://doi.org/10.1038/nature09467

Toffoletto, F., Sazykin, S., Spiro, R., & Wolf, R. (2003). Inner magnetospheric modeling with the rice convection model. In A. C.-L. Chian, I. H. Cairns, S. B. Gabriel, J. P. Goedbloed, T. Hada, M. Leubner, et al. (Eds.), *Advances in space environment research—volume I* (pp. 175–196). Springer Netherlands. https://doi.org/10.1007/978-94-007-1069-6_19

Vasyliunas, V. M. (1970). Mathematical models of magnetospheric convection and its coupling to the ionosphere. In B. M. McCormac (Ed.), *Particles and fields in the magnetosphere*. Astrophysics and space science library (Vol. 17, pp. 60–71). Dordrecht: Springer. https://doi.org/10.1007/978-94-010-3284-1_6

Vondrak, R., & Robinson, R. (1985). Inference of high-latitude ionization and conductivity from AE-C measurements of auroral electron fluxes. *Journal of Geophysical Research*, *90*, 7505–7512. https://doi.org/10.1029/ja090ia08p07505

Weiss, L. A., Thomsen, M. F., Reeves, G. D., & McComas, D. J. (1997). An examination of the Tsyganenko (T89a) field model using a database of two-satellite magnetic conjunctions. *Journal of Geophysical Research*, *102*(A3), 4911–4918. https://doi.org/10.1029/96JA02876

Wiltberger, M., Weigel, R. S., Lotko, W., & Fedder, J. A. (2009). Modeling seasonal variations of auroral particle precipitation in a global-scale magnetosphere-ionosphere simulation. *Journal of Geophysical Research*, *114*(A1), A01204. https://doi.org/10.1029/2008JA013108

Wing, S., Gkioulidou, M., Johnson, J. R., Newell, P. T., & Wang, C.-P. (2013). Auroral particle precipitation characterized by the substorm cycle. *Journal of Geophysical Research: Space Physics*, *118*, 1022–1039. https://doi.org/10.1002/jgra.50160

Wing, S., & Johnson, J. R. (2015). Theory and observations of upward field-aligned currents at the magnetopause boundary layer. *Geophysical Research Letters*, *42*, 9149–9155. https://doi.org/10.1002/2015GL065464

Wing, S., Khazanov, G. V., Sibeck, D. G., & Zesta, E. (2019). Low energy precipitating electrons in the diffuse aurorae. *Geophysical Research Letters*, *46*(7), 3582–3589. https://doi.org/10.1029/2019gl082383

Wolf, R. A. (1970). Effects of ionospheric conductivity on convective flow of plasma in the magnetosphere. *Journal of Geophysical Research*, *75*(25), 4677–4698. https://doi.org/10.1029/JA075i025p04677

Wolf, R. A., Harel, M., Spiro, R. W., Voigt, G.-H., Reiff, P. H., & Chen, C.-K. (1982). Computer simulation of inner magnetospheric dynamics for the magnetic storm of July 29, 1977. *Journal of Geophysical Research*, *87*, 5949–5962. https://doi.org/10.1029/JA087iA08p05949

Zhang, B., Lotko, W., Brambles, O., Wiltberger, M., & Lyon, J. (2015). Electron precipitation models in global magnetosphere simulations. *Journal of Geophysical Research: Space Physics*, *120*(2), 1035–1056. https://doi.org/10.1002/2014JA020615